ACS Macro Letters

pubs.acs.org/macroletters Letter

Solvent Annealing of Striped Ellipsoidal Block Copolymer Particles: Reversible Control over Lamellae Asymmetry, Aspect Ratio, and Particle Surface

Lucila Navarro, Andreas F. Thünemann, and Daniel Klinger*

Cite This: *ACS Macro Lett.* 2022, 11, 329−335 Read Online

ACCESS | Metrics & More | Article Recommendations | Supporting Information

ABSTRACT: Solvent annealing is a versatile tool to adjust the shape and morphology of block copolymer (BCP) particles. During this process, polar solvents are often used for block-selective swelling. However, such water-miscible solvents can induce (partial) solubilization of one block in the surrounding aqueous medium, thus, causing complex structural variations and even particle disassembly. To reduce the complexity in morphology control, we focused on toluene as a nonpolar polystyrene-selective solvent for the annealing of striped polystyrene-*b*-poly(2-vinylpyridine) (PS-*b*-P2VP) ellipsoids. The selective stretching of PS chains produces unique asymmetric lamellae structures, which translate to an increase in the particle aspect ratio after toluene evaporation. Complete reversibility is achieved by changing to chloroform as a nonselective solvent. Moreover, surfactants can be used to tune block-selective wetting of the particle surface during the annealing; for example, a PS shell can protect the internal lamellae structure from disassembly. Overall, this versatile postassembly process enables the tailoring of the structural features of striped colloidal ellipsoids by only using commercial BCPs and solvents.

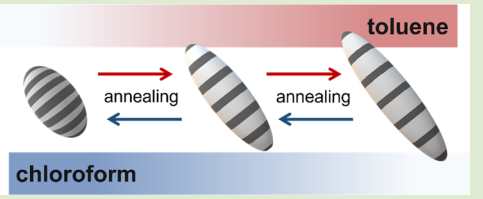

Shape anisotropic particles with defined internal nanostructures are promising building blocks for advanced applications in biology, photonics, catalysis, and so on.[1−4] To prepare such multifunctional colloids, evaporation-induced self-assembly of block copolymers (BCPs) has been established as a versatile method.[5] While the BCP volume ratio (packing parameter) determines the general morphology, the soft confinement of the emulsion droplets allows further structural variations. For this, various parameters can be adjusted during phase separation: the interfacial energies between BCP and the surrounding medium, the degree of confinement, the evaporation temperature, the pH of the continuous phase, and the evaporation kinetics.[6−11] In addition, the incorporation or removal of additives,[12] for example, different solvents,[13] small molecules,[14,15] homopolymers,[7,16,17] and even other (block) copolymers,[18,19] enable complex structures during particle preparation that can deviate from the pure BCP systems.

Alternatively, postassembly treatments allow adjusting shape and morphology of BCP particles after their preparation.[20−23] Among such strategies, (vapor) solvent annealing is a versatile residue-free method that is well-established for BCP thin films[24−27] but is still in its infancy for BCP particles. Here, current investigations often focus on controlling the domain orientation for a given underlying morphology. In colloidal systems, this can be achieved through varying the surfactants at the BCP/water interface.[20,21,28] For example, in particles with a lamellar morphology, a light-induced reversible shift between concentric-lamellar spheres and striped lamellar ellipsoids can be achieved by UV-responsive surfactants.[29,30] For such domain reorientations, a nonselective solvent is required to enable high mobility of both blocks without changing the BCP packing parameter during the annealing process.

In contrast, the utilization of block-selective solvents can actually change the underlying morphology by tuning the solubility and associated stretching of the individual BCP segments. The resulting variation of the BCP packing parameter induces a morphological transformation. This process strongly depends on the polarity and miscibility of the annealing solvent with the surrounding phase. In water, polar block-selective solvents can lead to a high swelling or even (partial) solubilization of one block, thus, causing structural variations and even disassembly.[31−33] For example, spherical polystyrene-*block*-poly(2-vinyl pyridine) (PS-*b*-P2VP) particles with concentric lamellae can transfer into vesicular structures upon the addition of ethanol as a highly polar P2VP-selective solvent.[22] Contrarily, nonpolar block selective solvents are less explored. Such water immiscible solvents selectively induce chain stretching in the respective domains. In combination with the less flexible nonswollen domains that can act as physical boundaries, complex morphological transformations can be induced. However, more investigations are needed to determine

Received: October 26, 2021
Accepted: February 8, 2022
Published: February 17, 2022

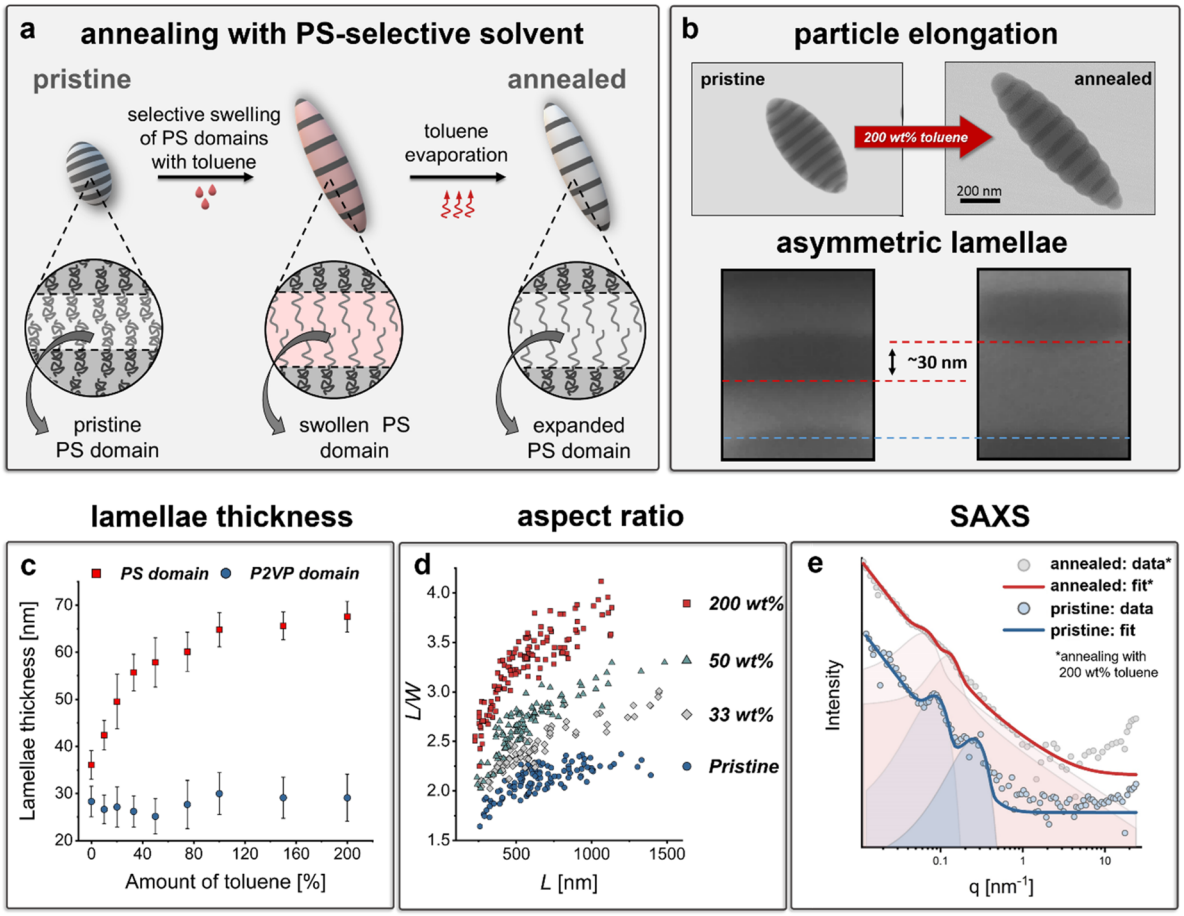

Figure 1. (a) Schematic representation of the particle solvent annealing process: Toluene as a selective solvent for the PS segments is added to a suspension of pristine PS-*b*-P2VP particles. The resulting stretching of the PS selectively increases the PS lamellae thickness and translates to particle elongation after solvent evaporation. (b) Comparing TEM images of pristine and annealed particles shows a particle elongation, that is, an increase in the aspect ratio for the same number of 10 lamellae per particle. The detailed pictures of the particles' the middle sections show an exclusive increment of approximately 30 nm in the PS thickness, thus, resulting in an asymmetric lamellae morphology. (c) While PS lamellae thickness increases with the amount of toluene in the annealing process, the P2VP lamellae thickness remains unchanged. (d) The aspect ratio of annealed particles increases with toluene (e.g., 33, 50, and 200 wt %) and depends on the particles' long axis, that is, the number of lamellae per particle. (e) Small angle X-ray scattering patterns of pristine and annealed particles (200 wt % of toluene) show an increase in domain spacing after annealing.

the potential of such strategies for tailoring BCP particle shape and morphology.

In addressing this need, we aim to investigate such phenomena in striped ellipsoidal particles. In such stacked lamellar structures, chain stretching can occur almost freely in the *z*-direction (perpendicular to the lamellae), that is, the influence of the nonswollen domains is minimized. Thus, selective swelling of one domain can translate to a particle elongation, that is, a change in aspect ratio while maintaining the lamellar morphology. While this is reported for cross-linked domains (via the addition of organic solvents[34] or pH changes[6]), the cross-linking points prevent the retention of chain stretching after solvent evaporation. Thus, the initial structure (as before "annealing") is restored in these cases. In un-cross-linked domains, it is assumed that this process is different. Here, the chains can remain stretched after solvent evaporation. However, since chain stretching is entropically unfavored, this either requires kinetic trapping or enthalpic compensation. In such cases, we hypothesize that the final annealed structure consists of asymmetric lamellae, that is, different BCP domains with different thicknesses (see Figure 1a). Targeting such asymmetric structures through established assembly methods would require complex miktoarm star copolymer architectures that are difficult to synthesize.[35] In contrast our suggested postassembly method is based on easily accessible commercial linear diblock copolymers and common solvents. Thus, this strategy would represent a facile and robust alternative to tailoring the aspect ratio and lamellar thickness of such colloidal ellipsoids.

To examine the effect of a selective nonpolar solvent on the morphology of lamellar BCP particles, we used striped PS-*b*-P2VP ellipsoids and toluene as a PS-selective solvent. The particles were prepared according to our previously published method that uses a mixed surfactant system to provide neutral wetting conditions for both blocks at the interphase.[6] After particle preparation, different amounts of toluene were directly added (via micropipette) to the dispersion of striped ellipsoids. By avoiding the uncontrolled transfer of the solvent from a vapor phase to the dispersion (as reported for vapor annealing processes), the toluene amount could be controlled precisely. After solvent addition, the mixtures were briefly sonicated to generate small droplets of toluene, thus, enhancing the solvent's surface to volume ratio and enable fast diffusion into the particles. Toluene amounts were gradually varied between 10 and 250 wt % with respect to the total mass of pristine particles. After a predetermined time for swelling, toluene was evaporated to obtain solid non-swollen particles.

https://doi.org/10.1021/acsmacrolett.1c00665
ACS Macro Lett. 2022, 11, 329−335

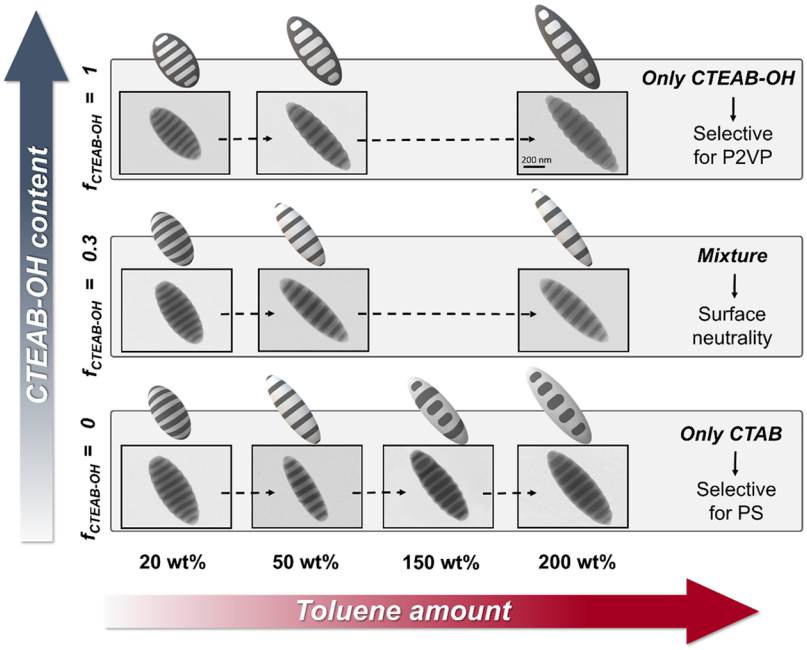

Figure 2. Influence of surfactants on the particle morphology after annealing with different amounts of toluene. By varying the composition of a surfactant mixture consisting of PS-selective CTAB and P2VP-selective CTEAB-OH, the wetting of the particle surface by the different BCP segments can be controlled. This depends on the amount of toluene, as the solvent is assumed to act as a plasticizer for the P2VP domains. Thus, high toluene contents above 150 wt % can induce a full P2VP (for pure CTEAB-OH) or PS (for pure CTAB) shell around the particles. A surfactant mixture with a CTEAB-OH content of 0.3 can ensure neutral wetting of the BC/water interface.

For increasing toluene content, transmission electron microscopy (TEM) revealed an exclusive increase of the PS domain thickness. This translates to an increase in aspect ratio (AR = L/W), that is, particle elongation (Figures 1, S1, and S2). The underlying process involves the selective expansion of the PS chains (due to their toluene affinity) and retention of the stretched conformation after evaporation (see Figure 1a). For annealing with 200 wt % of toluene, this phenomenon is most prominent and the PS lamellae thickness increased from 36 ± 5 nm (before annealing) to 67 ± 5 nm (after annealing; Figure 1b). Depending on the number of PS lamellae per particle, this can almost double the aspect ratio (Figure 1d). For example, a 1.7-fold increase from AR = 2.2 to 3.7 is observed for particles with 10 PS domains (Figure 1b). Since the P2VP domain thickness remains constant during this process (see Figures 1c and S1), the aspect ratio increment corresponds to a new asymmetric lamellar morphology with PS domains being thicker than P2VP domains.

The asymmetry of morphology and shape can be tuned precisely by varying the amount of toluene. Figure 1c shows a steep increase in PS domain thickness for toluene contents up to 100 wt %. For additional toluene amounts, a plateau is reached at a PS thickness of around 62−67 nm. In contrast, the thickness of the P2VP domains remains similar to the pristine particles. While these values were obtained from TEM analysis, we also aimed to evaluate the increase of lamellar domain spacing more quantitatively. For this, SAXS measurements were performed on pristine and highly swollen particles with 200 wt % of toluene (Figures 1e and S3). For pristine particles, the peak maxima are observed at q_1 = 0.08 nm^{-1} and q_2 = 0.252 nm^{-1} (indexed as (001) and (003) since $q_2 = 3q_1$). This translates to a domain spacing of $d = 2\pi/q_1 = d_{PS} + d_{P2VP}$ of 75 nm. In contrast, for the swollen particles, the peak maxima are observed at q_1 = 0.06 nm^{-1} and q_2 = 0.12 nm^{-1} (indexed as (001) and (002) since $q_2 = 2q_1$). Thus, the domain spacing for the swollen particles was 100 nm. Assuming that the P2VP thickness remains constant (as seen in TEM), the 25 nm increment can be attributed to an exclusive increase of PS thickness. This enlarged domain spacing from SAXS (+25 nm) correlates well with the value obtained from TEM (+30 nm), and slight differences are attributed to the error of manual measurements in TEM ($d_{pristine}$ = 66 ± 5 nm and $d_{swollen}$ = 95 ± 7 nm).

The increase of PS domain thickness increases the particle length (L). Since the width (W) remains constant, particle AR increases with toluene content (Figures 1d and S4). However, AR also varies with particle size, described by length (L). This correlation is already observed in the preparation of pristine particles and results from the thermodynamics of the BCP phase separation. Since surface energy influences ellipsoid formation, larger particles are easier to deform due to their lower surface to volume ratio.[6] As shown in Figure 1d, this trend is transferred to the annealed particles. For 33, 50, and 200 wt % toluene, the AR increases with L for each sample. Moreover, the AR difference between annealed and pristine particles is more pronounced for larger particles (for all samples see Figure S5).

Overall, this postassembly strategy is simple, robust, and mainly depends on the amount of toluene. To confirm this, we carefully screened the influence of other parameters, such as swelling temperature (Figure S6), swelling time (Figure S7), and toluene evaporation rate (Figure S8). These tests did not reveal any additional effect (see Table S2). Thus, aspect ratios up to AR = 4 and asymmetric morphologies with PS domains being double as thick as P2VP domains can be achieved by simply varying the toluene content between 0 and 200 wt %. However, exceeding 200 wt % can lead to a loss of the lamellar morphology. As shown in Figure S9, a complete rearrangement of the particles to a spherical shape with multiple P2VP centers is observed for toluene amounts of 250 wt %. This is assumed to be

https://doi.org/10.1021/acsmacrolett.1c00665
ACS Macro Lett. 2022, 11, 329−335

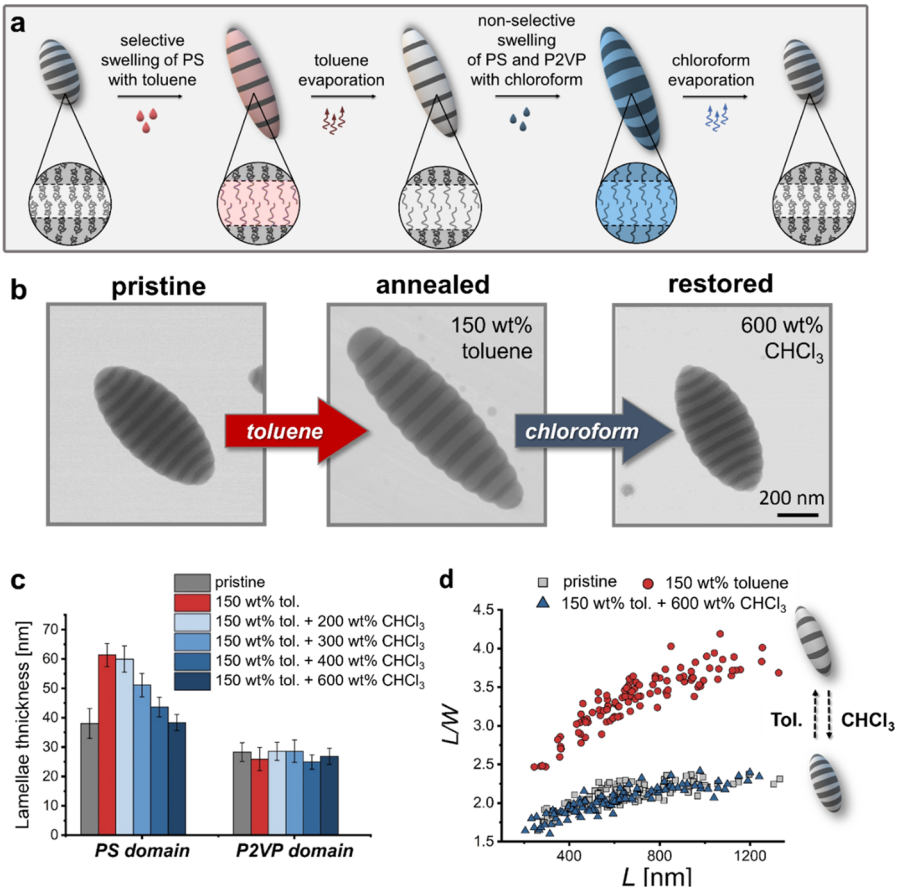

Figure 3. (a) Schematic representation showing the reversibility of the annealing process. An initial solvent annealing step with toluene as block-selective solvent will mainly expand the PS domains after evaporation. Subsequent swelling with chloroform, as a nonselective solvent for both domains, will equally mobilize both blocks and restore the initial particle shape and morphology after evaporation. (b) TEM pictures of particles at different stages of the process demonstrate the reversibility. Starting from pristine particles, PS-selective annealing with 150 wt % of toluene (at $f_{\mathrm{CTEAB\text{-}OH}} = 0.7$) leads to elongated particles with an increased thickness of PS domains. The initial structure can be restored by subsequent annealing with 600 wt % of chloroform. (c) PS and P2VP lamellae thicknesses for different amounts of chloroform show that restoration of the initial domain sizes requires at least 600 wt % of chloroform. (d) For elongated particles that were annealed with 150 wt % of toluene, the aspect ratio distribution of pristine particles can be completely restored by the subsequent annealing with 600 wt % of chloroform.

the result of P2VP plasticization by such large amounts of toluene.[36]

While this method allows accurate control over asymmetric lamellae morphologies, interpretation of the underlying annealing process is challenging. Overall, the entropically unfavored stretching of PS chains requires kinetic stabilization or energetic compensation. While fast vitrification of swollen domains could trap such energetically unfavored structures, the influence of evaporation rate on the morphology is negligible (Figure S8). Hence, we suggest enthalpic compensation due to structural changes at the BCP/water interface. Examining annealed particles in more detail, a thin layer of P2VP was observed to cover the particle surface (Figure S10). This suggests P2VP plasticization to allow partial migration of P2VP segments to the BCP/water interface. The preferential affinity of P2VP for the aqueous phase shows a disturbed balance of the neutral wetting conditions that are initially defined during preparation of the pristine particles.[37] Originally, a mixture of PS- and P2VP-selective surfactants (CTAB and CTEAB-OH, respectively) was carefully adjusted to the BCP volume ratio. However, during annealing, the PS domains expand and the corresponding surface area increases, that is, about +30% for annealing with 150 wt % toluene (see Figure S11). As a result, domain sizes do not match the initial surfactant ratio anymore, and the increased PS/water interface is energetically unfavored. We assume this effect is mediated by BCP rearrangements at the particle surface to cover the PS domains with P2VP. Since this reduces the PS/water interface, the corresponding enthalpic gain compensates for the entropically unfavored PS stretching.

These results suggest stabilization of the asymmetric lamellae through the BCP/water interface. Since this interface is governed by the surfactants, varying the surfactant ratio should enable further tuning of the final morphology. To investigate this influence, the pristine particles were first purified by cycles of centrifugation and redispersion in different surfactant mixtures before annealing with toluene. Figure 2 shows the variety of structures obtained for different contents of CTEAB-OH, denoted as the weight fraction $f_{\mathrm{CTEAB\text{-}OH}}$. An overview of the conditions is shown in Table S3, and additional TEM images are shown in Figures S12 and S13. In these experiments, a surfactant mixture with $f_{\mathrm{CTEAB\text{-}OH}} = 0.3$ provided neutral wetting of both blocks at the particle surface. Here, we assume that the excess of PS-selective CTAB (70 wt %) can stabilize the additional PS/water interface. Since no redistribution of P2VP occurs, the P2VP chains can also stretch and the lamellar asymmetry ($d_{\mathrm{PS}}/d_{\mathrm{P2VP}}$) is reduced (Figures S14 and S15). Simultaneous reduction of PS expansion suggests that stabilization of the PS surface with CTAB is less effective than by P2VP migration.

https://doi.org/10.1021/acsmacrolett.1c00665
ACS Macro Lett. 2022, 11, 329−335

These assumptions are further supported by control experiments using CTEAB-OH contents of $f_{CTEAB\text{-}OH}$ = 0.65 and 0.75 (close to the initial composition $f_{CTEAB\text{-}OH}$ = 0.70; Figures S10 and S13). Here, P2VP domains preferably interact with the excess CTEAB-OH, leading to partial engulfing of the PS domains. This P2VP redistribution then increases the lamellae asymmetry again (see Figures S14 and S15). Overall, these findings suggest that the additional PS surface can be stabilized either directly by using more PS-selective CTAB or indirectly by a partial migration of P2VP segments to engulf the PS domains and minimize the PS/water interface. In both cases, it is assumed that these favorable interactions can compensate the entropically unfavored stretching of the PS chains.

In addition to these mechanistic considerations, varying the surfactants also allows further tuning of the particle structure via annealing. It is assumed that a complete wetting of one block can be induced by resuspending the particles in a single surfactant solution. Indeed, by using a mass fraction of $f_{CTEAB\text{-}OH}$ of 1 (only CTEAB-OH) migration of P2VP to the particle surface is observed for all toluene amounts. As discussed above, this contributes to a large lamellar asymmetry (Figure S14). In contrast, a mass fraction of $f_{CTEAB\text{-}OH}$ of 0 (only CTAB, selective for PS) induced migration of PS to the particle surface. This process depends on the amount of toluene and the corresponding level of PS chain mobility. A total of 20 to 50 wt % of toluene is not enough to induce complete PS migration to the interface. Instead, both domains are wetting the interface equally. Increasing the toluene amount to 150 wt %, morphological changes become obvious. In an intermediate state, part of the PS is able to migrate to the interface, while still some P2VP lamellae are exposed to the surface. For 200 wt % of toluene, this transition is complete and particles are obtained that are fully covered with a PS layer. Interestingly, this PS migration can stabilize a certain extent of P2VP chain stretching to cause an inverted lamellar asymmetry $d_{P2VP} > d_{PS}$. These results deviate from established annealing processes with a nonselective "good" solvent for both blocks. In such cases, a preferential interaction of one block with the surrounding surfactants will result in onion-like particles. In contrast, the utilization of toluene as block-selective nonpolar solvent restricts the chain motion of both blocks. This only allows the migration of a single domain to the particle interface and keeps the striped ellipsoidal shape.

Such new morphologies exhibit a homogeneous particle surface chemistry, which governs their behavior in dispersion. For example, a surrounding PS layer provides structural stabilization of the lamellar morphology against disassembly. As shown for striped PS-*b*-P2VP particles, low pH values can protonate the P2VP blocks, thus, inducing their water solubility. As a result, the particles disassemble into PS discs with dangling P2VP chains. Now this effect can be controlled by changing the structure of the particles through a quick annealing step. To evaluate this approach, annealed particles with different morphologies were acidified to pH 2−3 and their structure was determined by TEM (Figure S16). For particles with a surrounding P2VP shell (annealed in the presence of CTEAB-OH), a low pH induced complete disassembly into discrete PS disks. In contrast, a PS surface (annealed in the presence of CTAB) prevents the disassembly. For intermediate morphologies (annealed in the presence of CTAB and CTEAB-OH mixtures), disassembly occurs on the P2VP lamellae facing the aqueous phase. Thus, varying the surfactants during the annealing process enhances the portfolio of simple methods that can be used to control the particle properties in dispersion.

Since toluene annealing is a physical process to induce spatial and conformational changes in the BCP chains, it should be reversible. Thus, an equal mobilization of both blocks under neutral wetting conditions should restore the initial shape and morphology upon solvent evaporation. For this, a good solvent for both blocks is required. To test this assumption, pristine particles were first annealed with 150 wt % of toluene to induce particle elongation upon stretching of the PS domains. Then, chloroform was added as a "good" solvent in different amounts and slowly evaporated (see Figure 3a). By examining the particle structures after the second annealing step, it was found that chloroform is able to induce morphological changes that are concentration-dependent. As shown by TEM images in Figure 3b, the particles' initial structure (AR and domain thickness) was completely restored for 600 wt % of chloroform (also see Figures S17 and S18). Between 200 and 600 wt % of added chloroform, the PS lamella thickness (Figure 3c) and the particle aspect ratio (Figures 3d and S13b) are progressively returning to their original values. These observations support our hypothesis of the underlying process and provide additional versatility to tune the particles' structure.

In summary, we have demonstrated a new postassembly strategy to control the shape and morphology of striped PS-*b*-P2VP ellipsoids. The block-selective solvent annealing process gives access to unique asymmetric domain structures and allows accurate control over four parameters: PS lamellar thickness, particle aspect ratio, domain orientation at the BCP/water interphase, and reversibility. A key benefit of this process is the ability to gradually change the particles' structural features by solely adjusting the amount of solvent. This highlights the simplicity and the robustness of this process. Using toluene as a PS-selective nonpolar solvent enables asymmetric lamellae with the PS domains being roughly double the size as the P2VP domains. This translates into particle elongation and an increase of aspect ratio. Depending on the number of lamellae per particle, AR can almost double to values of almost 4. In addition, the domain orientation at the particle surface can be controlled through the surfactants. This enables to select a single domain to cover the entire particle surface and protect the internal lamellar structure from disassembly. Finally, complete reversibility is achieved by changing the annealing solvent to a nonselective solvent. Overall, the process represents a new synthetic tool to access a variety of new structures from a single batch of preformed particles.

■ ASSOCIATED CONTENT

Supporting Information

The Supporting Information is available free of charge at https://pubs.acs.org/doi/10.1021/acsmacrolett.1c00665.

Description of materials, synthetic procedures, and characterization methods. Small-angle X-ray scattering (SAXS): experimental procedure, peak fitting, and data processing. Experimental procedure for particle synthesis and annealing. Supporting figures: TEM images for annealed particles, SAXS patterns with all fits, analysis of particle shape (length, width, aspect ratio), influence of annealing conditions (temperature, time, evaporation rate), particle surface areas and lamellar asymmetry, reversibility of annealing (PDF)

https://doi.org/10.1021/acsmacrolett.1c00665
ACS Macro Lett. 2022, 11, 329−335

AUTHOR INFORMATION

Corresponding Author

Daniel Klinger − *Institute of Pharmacy (Pharmaceutical Chemistry), Freie Universität Berlin, 14195 Berlin, Germany;* orcid.org/0000-0002-8876-5088; Email: daniel.klinger@fu-berlin.de

Authors

Lucila Navarro − *Institute of Pharmacy (Pharmaceutical Chemistry), Freie Universität Berlin, 14195 Berlin, Germany*

Andreas F. Thünemann − *Bundesanstalt für Materialforschung und -prüfung (BAM), 12205 Berlin, Germany;* orcid.org/0000-0002-9883-6134

Complete contact information is available at: https://pubs.acs.org/10.1021/acsmacrolett.1c00665

Notes

The authors declare no competing financial interest.

ACKNOWLEDGMENTS

The authors would like to thank Glen J. Smales for the help in SAXS measurements. L.N. acknowledges the funding from the European Union's Horizon 2020 research and innovation programme under the Marie Skłodowska-Curie Grant agreement No. 838448. We would like to acknowledge the assistance of the Core Facility BioSupraMol supported by the DFG.

REFERENCES

(1) Shin, J. J.; Kim, E. J.; Ku, K. H.; Lee, Y. J.; Hawker, C. J.; Kim, B. J. 100th Anniversary of Macromolecular Science Viewpoint: Block Copolymer Particles: Tuning Shape, Interfaces, and Morphology. *ACS Macro Lett.* **2020**, *9* (3), 306−317.

(2) Chen, C.; Wylie, R. A. L.; Klinger, D.; Connal, L. A. Shape Control of Soft Nanoparticles and Their Assemblies. *Chem. Mater.* **2017**, *29* (5), 1918−1945.

(3) He, Q.; Ku, K. H.; Vijayamohanan, H.; Kim, B. J.; Swager, T. M. Switchable Full-Color Reflective Photonic Ellipsoidal Particles. *J. Am. Chem. Soc.* **2020**, *142* (23), 10424−10430.

(4) Varadharajan, D.; Turgut, H.; Lahann, J.; Yabu, H.; Delaittre, G. Surface-Reactive Patchy Nanoparticles and Nanodiscs Prepared by Tandem Nanoprecipitation and Internal Phase Separation. *Adv. Funct. Mater.* **2018**, *28* (39), 1800846.

(5) Ku, K. H.; Shin, J. M.; Yun, H.; Yi, G.-R.; Jang, S. G.; Kim, B. J. Multidimensional Design of Anisotropic Polymer Particles from Solvent-Evaporative Emulsion. *Adv. Funct. Mater.* **2018**, *28* (42), 1802961.

(6) Klinger, D.; Wang, C. X.; Connal, L. A.; Audus, D. J.; Jang, S. G.; Kraemer, S.; Killops, K. L.; Fredrickson, G. H.; Kramer, E. J.; Hawker, C. J. A Facile Synthesis of Dynamic, Shape-Changing Polymer Particles. *Angew. Chem., Int. Ed.* **2014**, *53* (27), 7018−7022.

(7) Jeon, S.-J.; Yi, G.-R.; Yang, S.-M. Cooperative Assembly of Block Copolymers with Deformable Interfaces: Toward Nanostructured Particles. *Adv. Mater.* **2008**, *20* (21), 4103−4108.

(8) Steinhaus, A.; Pelras, T.; Chakroun, R.; Gröschel, A. H.; Müllner, M. Self-Assembly of Diblock Molecular Polymer Brushes in the Spherical Confinement of Nanoemulsion Droplets. *Macromol. Rapid Commun.* **2018**, *39* (19), 1800177.

(9) Yabu, H.; Higuchi, T.; Shimomura, M. Unique Phase-Separation Structures of Block-Copolymer Nanoparticles. *Adv. Mater.* **2005**, *17* (17), 2062−2065.

(10) Shin, J. M.; Kim, Y.; Yun, H.; Yi, G.-R.; Kim, B. J. Morphological Evolution of Block Copolymer Particles: Effect of Solvent Evaporation Rate on Particle Shape and Morphology. *ACS Nano* **2017**, *11* (2), 2133−2142.

(11) Lee, J.; Ku, K. H.; Park, C. H.; Lee, Y. J.; Yun, H.; Kim, B. J. Shape and Color Switchable Block Copolymer Particles by Temperature and pH Dual Responses. *ACS Nano* **2019**, *13* (4), 4230−4237.

(12) Xu, J.; Yang, Y.; Wang, K.; Li, J.; Zhou, H.; Xie, X.; Zhu, J. Additives Induced Structural Transformation of ABC Triblock Copolymer Particles. *Langmuir* **2015**, *31* (40), 10975−10982.

(13) Deng, R.; Zheng, L.; Mao, X.; Li, B.; Zhu, J. Transformable Colloidal Polymer Particles with Ordered Internal Structures. *Small* **2021**, *17* (4), 2006132.

(14) Lee, S.; Shin, J. J.; Ku, K. H.; Lee, Y. J.; Jang, S. G.; Yun, H.; Kim, B. J. Interfacial Instability-Driven Morphological Transition of Prolate Block Copolymer Particles: Striped Football, Larva to Sphere. *Macromolecules* **2020**, *53* (16), 7198−7206.

(15) Klinger, D.; Robb, M. J.; Spruell, J. M.; Lynd, N. A.; Hawker, C. J.; Connal, L. A. Supramolecular guests in solvent driven block copolymer assembly: from internally structured nanoparticles to micelles. *Polym. Chem.* **2013**, *4* (19), 5038−5042.

(16) Schmidt, B. V. K. J.; Elbert, J.; Scheid, D.; Hawker, C. J.; Klinger, D.; Gallei, M. Metallopolymer-Based Shape Anisotropic Nanoparticles. *ACS Macro Lett.* **2015**, *4* (7), 731−735.

(17) Okubo, M.; Saito, N.; Takekoh, R.; Kobayashi, H. Morphology of polystyrene/polystyrene-block-poly(methyl methacrylate)/poly(methyl methacrylate) composite particles. *Polymer* **2005**, *46* (4), 1151−1156.

(18) Grundy, L. S.; Lee, V. E.; Li, N.; Sosa, C.; Mulhearn, W. D.; Liu, R.; Register, R. A.; Nikoubashman, A.; Prud'homme, R. K.; Panagiotopoulos, A. Z.; Priestley, R. D. Rapid Production of Internally Structured Colloids by Flash Nanoprecipitation of Block Copolymer Blends. *ACS Nano* **2018**, *12* (5), 4660−4668.

(19) Kim, E. J.; Shin, J. M.; Kim, Y.; Ku, K. H.; Yun, H.; Kim, B. J. Shape control of nanostructured cone-shaped particles by tuning the blend morphology of A-b-B diblock copolymers and C-type copolymers within emulsion droplets. *Polym. Chem.* **2019**, *10* (19), 2415−2423.

(20) Deng, R.; Liang, F.; Li, W.; Yang, Z.; Zhu, J. Reversible Transformation of Nanostructured Polymer Particles. *Macromolecules* **2013**, *46* (17), 7012−7017.

(21) Shin, J. M.; Lee, Y. J.; Kim, M.; Ku, K. H.; Lee, J.; Kim, Y.; Yun, H.; Liao, K.; Hawker, C. J.; Kim, B. J. Development of Shape-Tuned, Monodisperse Block Copolymer Particles through Solvent-Mediated Particle Restructuring. *Chem. Mater.* **2019**, *31* (3), 1066−1074.

(22) Fan, H.; Jin, Z. Selective Swelling of Block Copolymer Nanoparticles: Size, Nanostructure, and Composition. *Macromolecules* **2014**, *47* (8), 2674−2681.

(23) Mei, S.; Jin, Z. Mesoporous Block-Copolymer Nanospheres Prepared by Selective Swelling. *Small* **2013**, *9* (2), 322−329.

(24) Son, J. G.; Gotrik, K. W.; Ross, C. A. High-Aspect-Ratio Perpendicular Orientation of PS-b-PDMS Thin Films under Solvent Annealing. *ACS Macro Lett.* **2012**, *1* (11), 1279−1284.

(25) Sinturel, C.; Vayer, M.; Morris, M.; Hillmyer, M. A. Solvent Vapor Annealing of Block Polymer Thin Films. *Macromolecules* **2013**, *46* (14), 5399−5415.

(26) Baruth, A.; Seo, M.; Lin, C. H.; Walster, K.; Shankar, A.; Hillmyer, M. A.; Leighton, C. Optimization of Long-Range Order in Solvent Vapor Annealed Poly(styrene)-block-poly(lactide) Thin Films for Nanolithography. *ACS Appl. Mater. Interfaces* **2014**, *6* (16), 13770−13781.

(27) Montarnal, D.; Delbosc, N.; Chamignon, C.; Virolleaud, M.-A.; Luo, Y.; Hawker, C. J.; Drockenmuller, E.; Bernard, J. Highly Ordered Nanoporous Films from Supramolecular Diblock Copolymers with Hydrogen-Bonding Junctions. *Angew. Chem., Int. Ed.* **2015**, *54* (38), 11117−11121.

(28) Qiang, X.; Dai, X.; Steinhaus, A.; Gröschel, A. H. Multicompartment Microparticles with Patchy Topography through Solvent-Adsorption Annealing. *ACS Macro Lett.* **2019**, *8* (12), 1654−1659.

(29) Lee, J.; Ku, K. H.; Kim, M.; Shin, J. M.; Han, J.; Park, C. H.; Yi, G.-R.; Jang, S. G.; Kim, B. J. Stimuli-Responsive, Shape-Transforming Nanostructured Particles. *Adv. Mater.* **2017**, *29* (29), 1700608.

(30) Lee, J.; Ku, K. H.; Kim, J.; Lee, Y. J.; Jang, S. G.; Kim, B. J. Light-Responsive, Shape-Switchable Block Copolymer Particles. *J. Am. Chem. Soc.* **2019**, *141* (38), 15348−15355.
(31) Mei, S.; Jin, Z. Mesoporous Block-Copolymer Nanospheres Prepared by Selective Swelling. *Small* **2013**, *9* (2), 322−329.
(32) Steinhaus, A.; Chakroun, R.; Müllner, M.; Nghiem, T.-L.; Hildebrandt, M.; Gröschel, A. H. Confinement Assembly of ABC Triblock Terpolymers for the High-Yield Synthesis of Janus Nanorings. *ACS Nano* **2019**, *13* (6), 6269−6278.
(33) Deng, R.; Liang, F.; Zhou, P.; Zhang, C.; Qu, X.; Wang, Q.; Li, J.; Zhu, J.; Yang, Z. Janus Nanodisc of Diblock Copolymers. *Adv. Mater.* **2014**, *26* (26), 4469−4472.
(34) Schmidt, B. V. K. J.; Wang, C. X.; Kraemer, S.; Connal, L. A.; Klinger, D. Highly functional ellipsoidal block copolymer nanoparticles: a generalized approach to nanostructured chemical ordering in phase separated colloidal particles. *Polym. Chem.* **2018**, *9* (13), 1638−1649.
(35) Seo, Y.; Woo, D.; Li, L.; Li, W.; Kim, J. K. Phase Behavior of PS-(PS-b-P2VP)3 Miktoarm Star Copolymer. *Macromolecules* **2021**, *54* (17), 7822−7829.
(36) Tashiro, K.; Yoshioka, A. Molecular Mechanism of Solvent-Induced Crystallization of Syndiotactic Polystyrene Glass. 2. Detection of Enhanced Motion of the Amorphous Chains in the Induction Period of Crystallization. *Macromolecules* **2002**, *35* (2), 410−414.
(37) Ren, M.; Hou, Z.; Zheng, X.; Xu, J.; Zhu, J. Electrostatic Control of the Three-Dimensional Confined Assembly of Charged Block Copolymers in Emulsion Droplets. *Macromolecules* **2021**, *54* (12), 5728−5736.

https://doi.org/10.1021/acsmacrolett.1c00665
ACS Macro Lett. 2022, 11, 329−335